Proposal to JLab PAC 53

Double Deeply Virtual Compton Scattering with SoLIDμ spectrometer

Zhiwen Zhao

SoLID Collaboration Meeting

June 7-8, 2025

Duke University

Jefferson Lab
Thomas Jefferson National Accelerator Facility

Proposal to PAC53 PR12-25-010

Proposal to JLab PAC 53

Double Deeply Virtual Compton Scattering with SoLIDμ spectrometer

Xinzhan Bai*, Alexandre Camsonne*†, Silviu Covrig Dusa, Kondo Gnanvo, Dave Mack, Michael McCaughan, and Richard Tyson

Thomas Jefferson National Accelerator Facility, Newport News, VA, USA

Juan-Sebastian Alvarado*, Raphaël Dupré, Adam Hobart, Dominique Marchand, Carlos Muñoz Camacho, Silvia Niccolai, and Eric Voutier*

Université Paris-Saclay, CNRS/IN2P3/IJCLab, Orsay, France

Haiyan Gao, Yining Liu, Bo Yu, Yi Yu, Zhiwen Zhao*, and Jingyi Zhou

Duke University, Durham, NC, USA

Keagan Bell, Debaditya Biswas, Marie Boër*, Gyang Chung, Mahmoud Gomina, Arna Ma, and Kemal Tezgin

Virginia Tech, Blacksburg, VA, USA

Garth Huber, Nathan Heinrich, Muhammad Junaid, Vijay Kumar, and Alicia Postuma

University of Regina, Regina, SK, Canada

Ronald Gilman

Rutgers University, Piscataway, NJ, USA

Nilanga Linayage, Huong Thi Nguyen, and Asar Ahmed

University of Virginia, Charlottesville, VA, USA

Yi Wang, Junhuai Xu, Zhihong Ye, Haojie Zhang, and Yaopeng Zhang

Tsinghua University, Beijing, China

Evaristo Cisbani

Istituto Superiore di Sanità, Roma, Italia

Guido Maria Urciuoli

INFN, Sezione di Roma1, Roma, Italia

Vincenzo Bellini and Concetta Maria Sutera

Università di Catania, Catania, Italia

Anthony W. Thomas

ARC Special Research Centre for the Subatomic Structure of Matter (CSSM), University of Adelaïde, Adelaïde, Australia

Pierre Chatagnon[1], Maxime Defurne[1], Víctor Martínez-Fernández[1,2], Hervé Moutarde[1], and Franck Sabatié[1]

[1] *IRFU, CEA, Université Paris-Saclay, Gif-sur-Yvette, France*

[2] *Center for Frontiers in Nuclear Science, Stony Brook University, Stony Brook, NY, USA*

Malek Mazouz and Wassim Hamdi

Faculté des Sciences de Monastir, Département de Physique, Monastir, Tunisia

Whitney Armstrong, Sylvester Joosten, and Zein-Eddine Meziani

Argonne National Laboratory, Physics Division, Argonne, IL, USA

Thomas Hemmick

Stony Brook University, Stony Brook, NY, USA

Bernard Pire

Centre de Physique Théorique, CNRS, École polytechnique, I.P. Paris, Palaiseau, France

Pawel Sznajder and Jakub Wagner

National Centre for Nuclear Research, NCBJ, Warsaw, Poland

Johan A. Colorado-Caicedo

Centro de Investigacion y de Estudios Avanzados del Instituto Politecnico Nacional,San Pedro Zacatenco, Mexico City, Mexico

Sudip Bhattarai

Idaho State University,Pocatello, ID, USA

Nikos Sparveris, Hamza Atac, Suman Shrestha, and Mazmus. Ifat

Temple University, Philadelphia, PA, USA

Mostafa Elaasar

Southern University at New Orleans,New Orleans, LA,USA

Darko Androić

University of Zagreb, Faculty of Science, Zagreb, Croatia

Eric Fuchey

College of William & Mary, Williamsburg, Virginia, USA

Hem Bhatt

Mississippi State University, Mississippi State, MS, USA

Pawel Nadel-Turonski

University of South Carolina, Columbia, SC, USA

Xiaqing Li, Tianbo Liu, and Weizhi Xiong

Shandong University, Qingdao, Shandong, China

*: Co-spokesperson, †: Contact-spokesperson (camsonne@jlab.org)

And SoLID Collaboration

Spokesperson : Juan-Sebastian Alvarado, Alexandre Camsonne, Marie Boer, Eric Voutier, Xinzhan Bai, Zhiwen Zhao

Overview

- General Parton Distribution
- Double Deeply Virtual Compton Scattering
- SoLIDμ setup
- Muon detector
- Simulation study
- Physics projections
- Beam time request
- Summary

Generalized Parton Distribution (GPD)

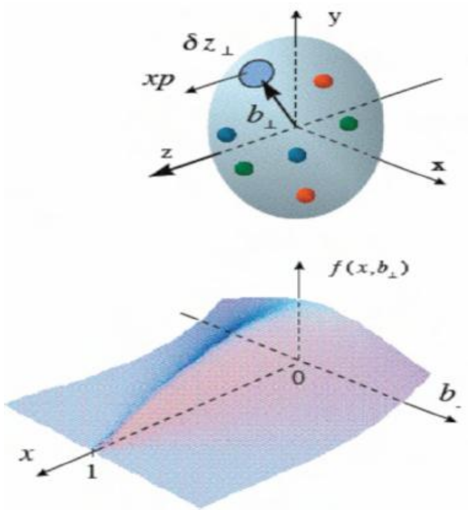

A unified descriptions of partons (quarks and gluons) in the momentum and impact parameter space

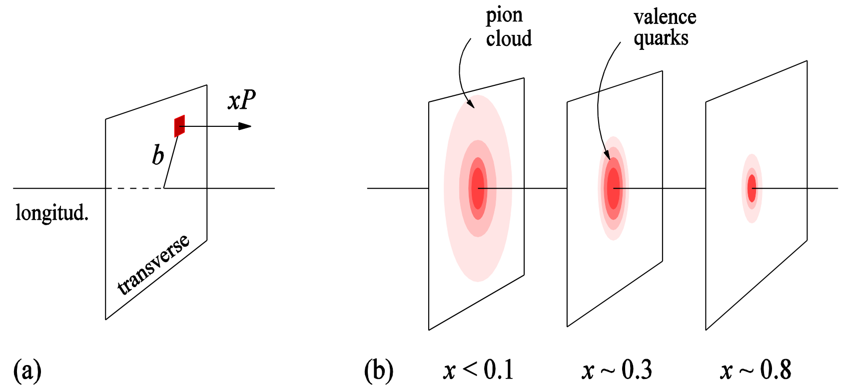

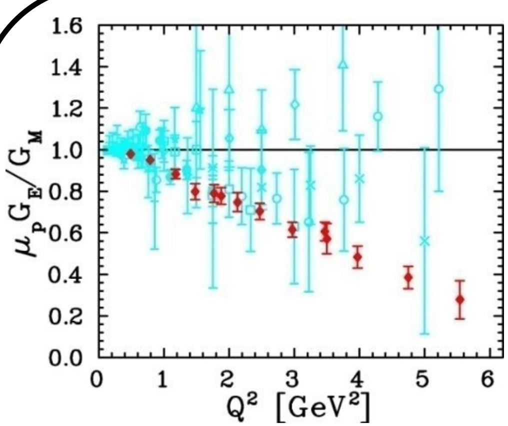

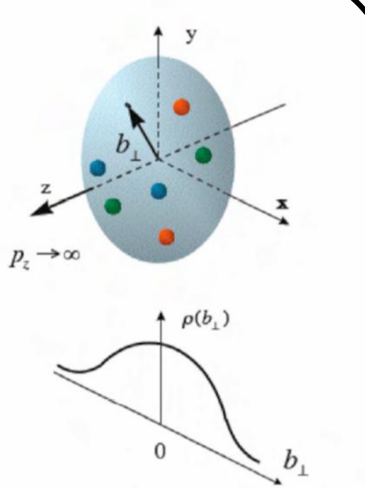

Elastic form factors

Transverse spatial distributions

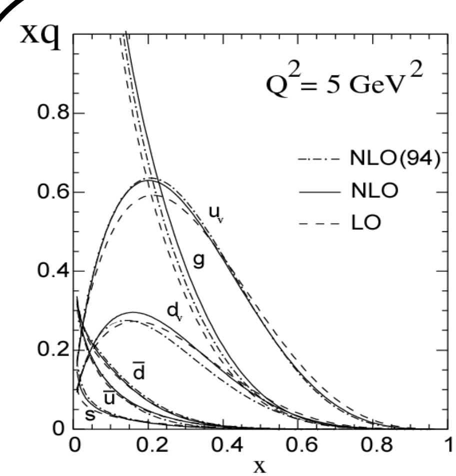

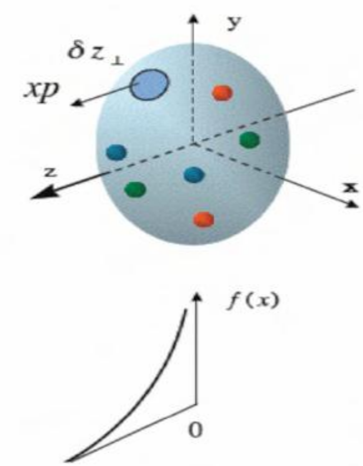

Parton Distribution Functions

Longitudinal momentum distributions

General Compton Process accessing GPD

$\gamma^*(q) + p(p) \rightarrow \gamma^*(q') + p(p')$

$$Q^2 = -q^2, \quad Q'^2 = q'^2, \quad s = (p+q)^2, \quad t = \Delta^2,$$

Deeply Virtual CS **($\gamma' \rightarrow \gamma$, $Q'^2=0$, $\xi' = \xi$)**
Timelike CS **($\gamma \rightarrow \gamma'$, $Q^2=0$, $\xi' = -\xi$)**
Double DVCS **($\gamma' \rightarrow \gamma'$)**

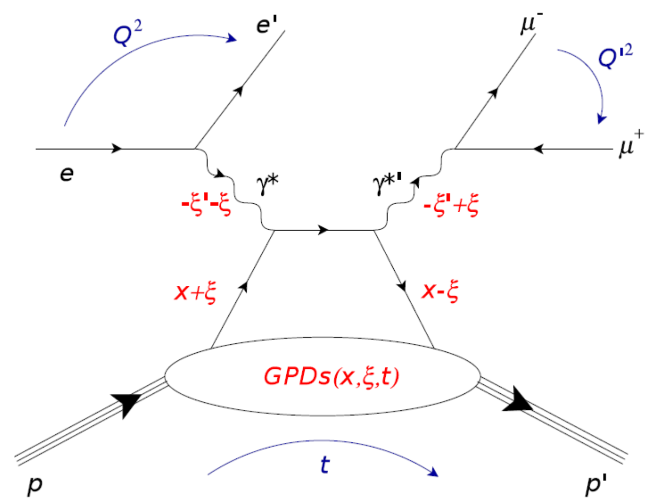

Because of the virtuality of the final photon, **DDVCS** allows a direct access to GPDs at $x \neq \pm\xi$, which is of importance for their modeling and for the investigation of **nuclear dynamics**.

Compton Form Factor (CFF)

$$\mathcal{F}(\xi', \xi, t) = \mathcal{P}\int_{-1}^{1} F_+(x, \xi, t)\left[\frac{1}{x-\xi'} \pm \frac{1}{x+\xi'}\right]dx - i\pi F_+(\xi', \xi, t)$$

GPD combination

$$F_+(x, \xi, t) = \sum_q \left(\frac{e_q}{e}\right)^2 \left[F^q(x, \xi, t) \mp F^q(-x, \xi, t)\right]$$

Generalized Bjorken variable $\quad \xi' = \dfrac{Q^2 - Q'^2 + t/2}{2Q^2/x_B - Q^2 - Q'^2 + t}$

Skewness $\quad \xi = \dfrac{Q^2 + Q'^2}{2Q^2/x_B - Q^2 - Q'^2 + t}$

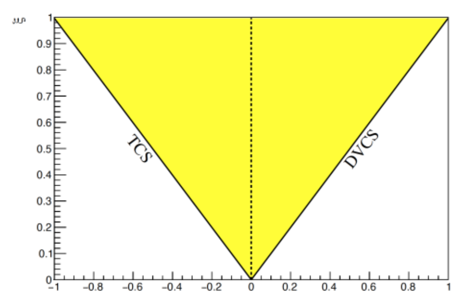

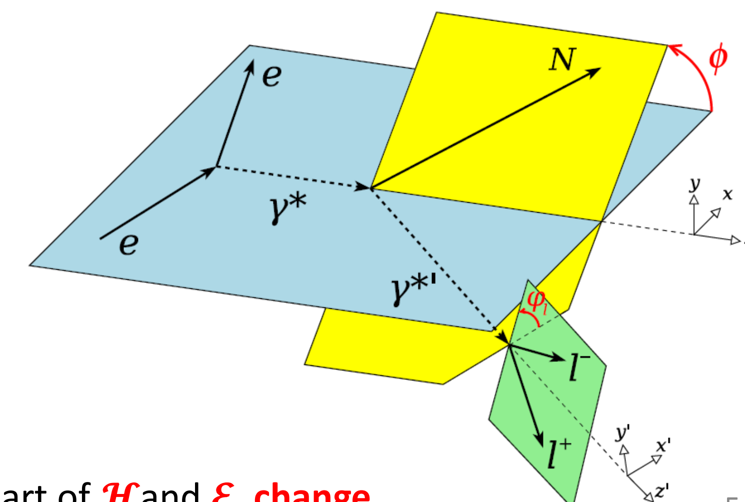

- Following the sign change of ξ' around $Q'^2=Q^2$, the imaginary part of $\mathcal{H}$ and $\mathcal{E}$ **change sign**, providing a testing ground of **GPD universality**.

Nucleon Femtography

M. Burkardt PRD 62 (2000) 071503. M. Diehl EPJC 25 (2002) 223 A.V. Belitsky, D. Müller, NPA 711 (2002) 118c J.P. Ralston; B. Pire PRD 66 (2002) 111501

$$\rho_H^q(x, \boldsymbol{b}_\perp) = \int \frac{d^2\boldsymbol{\Delta}_\perp}{(2\pi)^2}\, e^{i\boldsymbol{b}_\perp\cdot\boldsymbol{\Delta}_\perp}\,[H^q(x,0,-\Delta_\perp^2) + H^q(-x,0,-\Delta_\perp^2)]$$

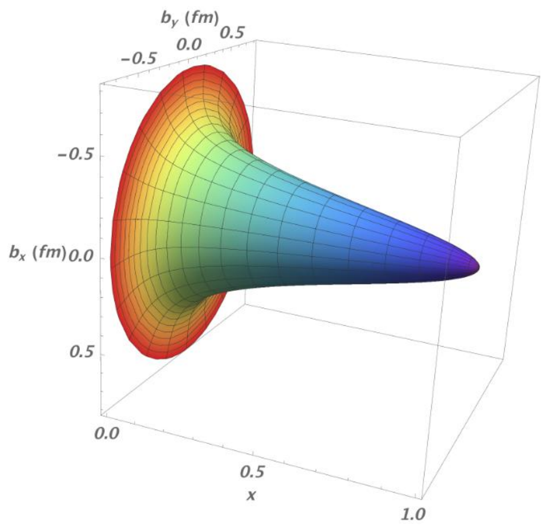

- The **transverse densities** of partons in nucleons and nuclei is related to the transverse momentum transfer ($-\Delta_\perp^2$) dependence of GPDs at **zero-skewness**.
- **DVCS** and **TCS cannot map out zero-skewness GPDs** over the **full physics phase space**.

The **experimental knowledge** of the **ξ-dependence** of GPDs at fixed longitudinal momentum fraction allows to **control** the **zero-skewness extrapolation** required for **nucleon imaging**.

R. Dupré, M. Guidal, M. Vanderhaeghen, PRD 95 (2017) 011501

Nucleon Spin

$$\boxed{\lim_{t\to 0}\int_{-1}^{1} x\,[H^q(x,\xi,t)+E^q(x,\xi,t)]\,dx = J^q}$$

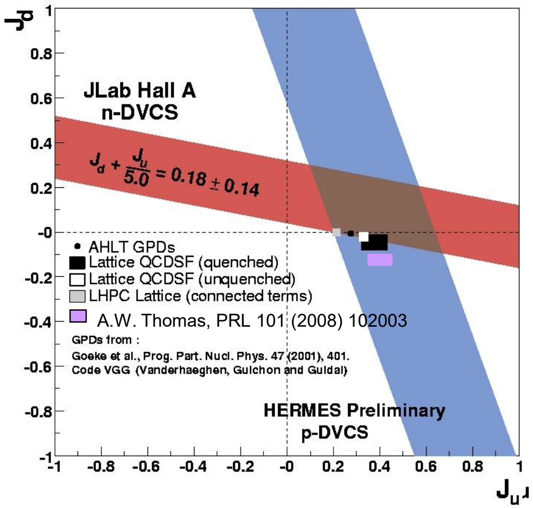

- The **total angular momentum of partons** inside the nucleon can be inferred from the Ji sum rule which involves the **forward limit** of the **first Mellin moment** of partons helicity conserving GPDs.
- **DVCS** and **TCS cannot access GPDs at $x \neq \xi$** over the **full physics phase space**.

> The **experimental knowledge** of the **ξ-dependence** of GPDs at fixed longitudinal momentum fraction is a **mandatory step for** unraveling the **nucleon spin**.

Nucleon Forces

$$\boxed{\int_{-1}^{1} x \sum_q H^q(x,\xi,t)\ dx = \ M_2(t) + \frac{4}{5}\xi^2 d_1(t)}$$

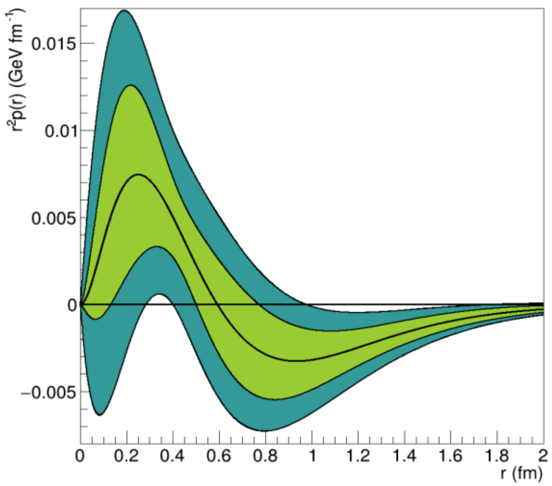

- The **skewness dependence** of the **first Mellin moment** of the GPD H provides an access to the **gravitational form factors** of the energy momentum tensor of the nucleon.
- $e^{\pm}$**-DVCS** and **TCS** offers another path via **dispersion relations**.

The **ξ-dependence** of GPDs reveals the **internal dynamics** of the nucleon.

V. Burkert, L. Elouadrhiri, F.-X. Girod, Nat. 557 (2018) 396; arXiv:2104.02031

Elementary Cross Section

DDVCS cross section is about 1/100 of DVCS and involves two Bethe-Heitler

$$d^7\sigma_P^e = d^7\sigma_{BH_1} + d^7\sigma_{BH_2} + d^7\sigma_{DDVCS} + P\, d^7\tilde{\sigma}_{DDVCS} + d^7\sigma_{INT_2} + P\, d^7\tilde{\sigma}_{INT_2} - e\left[d^7\sigma_{BH_{12}} + d^7\sigma_{INT_1} + P\, d^7\tilde{\sigma}_{INT_1}\right]$$

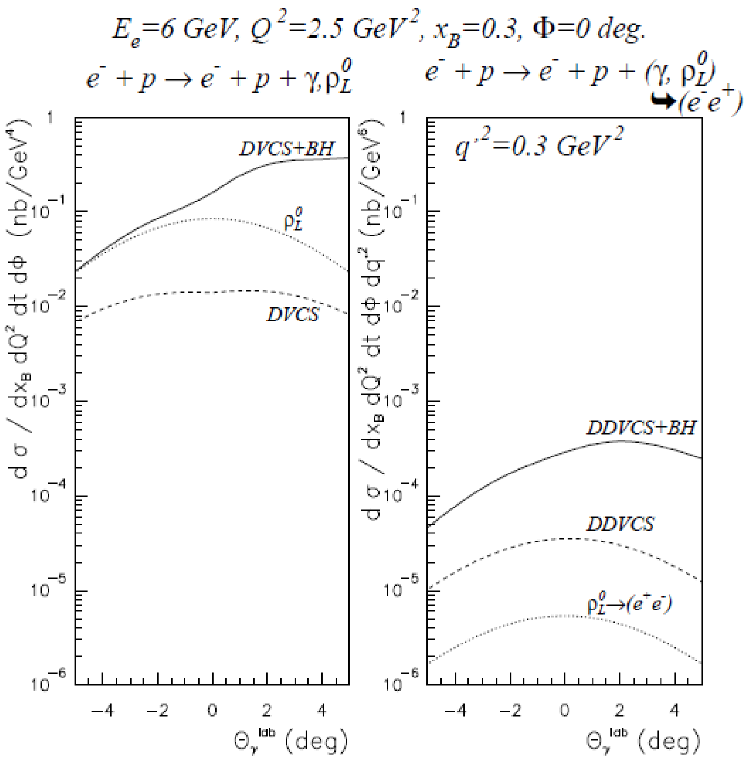

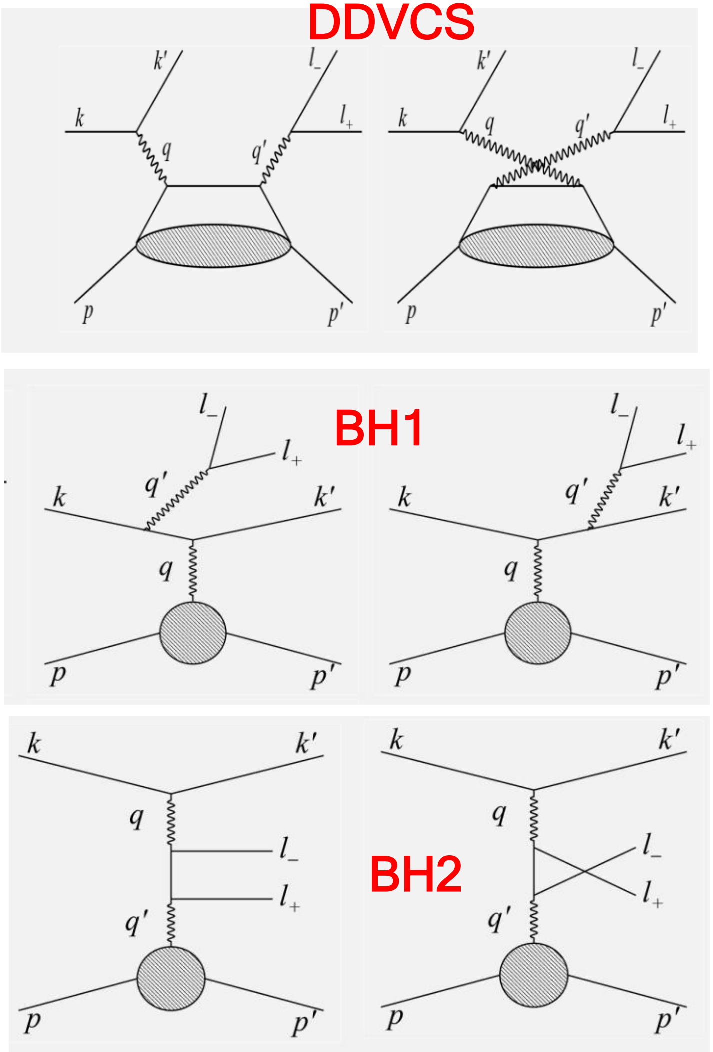

Integrated Cross Section

5-fold observables obtained from the integration over the polar angle of the muon and the azimuthal angle of the final virtual photon or the initial virtual photon are required, also minimizing the contribution of the BH_2 process.

DVCS-like

$$d^5\sigma^\lambda(\phi) \equiv \frac{d^5\sigma^\lambda(\phi)}{dx_B\, dy\, dt\, dQ'^2\, d\phi} = \int_0^{2\pi} d\varphi_\mu \int_{\pi/2-\theta_0}^{\pi/2+\theta_0} d\theta_\mu \sin(\theta_\mu)\, \frac{d^7\sigma^\lambda(\phi,\theta_\mu,\phi_\mu)}{dx_B\, dy\, dt\, d\phi\, dQ'^2\, d\Omega_\mu}$$

$$d^5\sigma^\lambda = d^5\sigma_{BH_1} + d^5\sigma_{BH_2} + d^5\sigma_{DDVCS} + d^5\sigma_{\mathcal{I}_1} + \lambda\, d^5\widetilde{\sigma}_{\mathcal{I}_1} = d^5\sigma_{UU} + \lambda\, d^5\sigma_{LU}$$

TCS-like

$$d^5\Sigma^\lambda(\varphi_\mu) \equiv \frac{d^5\sigma^\lambda(\varphi_\mu)}{dx_B\, dy\, dt\, dQ'^2\, d\varphi_\mu} = \int_0^{2\pi} d\phi \int_{\pi/2-\theta_0}^{\pi/2+\theta_0} d\theta_\mu \sin(\theta_\mu)\, \frac{d^7\sigma^\lambda(\phi,\theta_\mu,\phi_\mu)}{dx_B\, dy\, dt\, d\phi\, dQ'^2\, d\Omega_\mu}$$

$$d^5\Sigma^\lambda = d^5\Sigma_{BH_1} + d^5\Sigma_{BH_2} + d^5\Sigma_{BH_{12}} + d^5\Sigma_{DDVCS} + d^5\Sigma_{\mathcal{I}_1} + d^5\Sigma_{\mathcal{I}_2} + \lambda\, d^5\widetilde{\Sigma}_{\mathcal{I}_2} = d^5\Sigma_{UU} + \lambda\, d^5\Sigma_{LU}$$

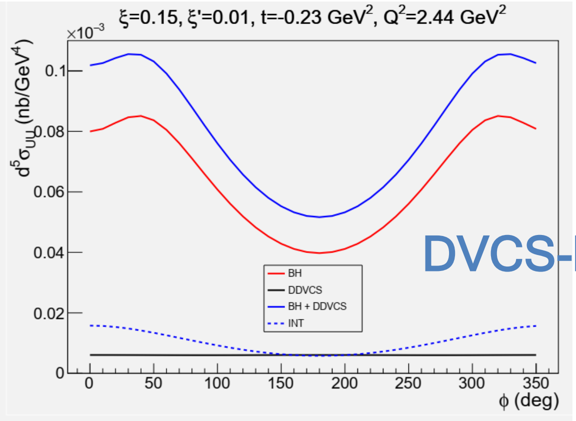

DVCS-like

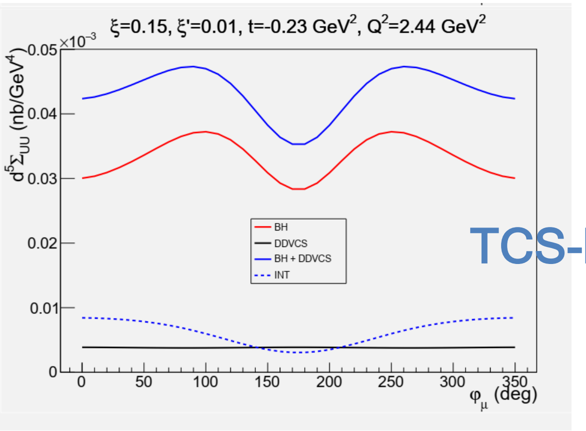

TCS-like

Beam Spin Asymmetry

$$A_{LU}^{\sigma^\lambda} \equiv A_{LU}^{\sigma^\lambda}(\phi) = \lambda\,\frac{d^5\sigma^+ - d^5\sigma^-}{d^5\sigma^+ + d^5\sigma^-} = \frac{\lambda\, d^5\widetilde{\sigma}_{\mathcal{I}_1}}{d^5\sigma_{BH_1} + d^5\sigma_{BH_2} + d^5\sigma_{DDVCS} + d^5\sigma_{\mathcal{I}_1}} \tag{29}$$

$$A_{LU}^{\Sigma^\lambda} \equiv A_{LU}^{\Sigma^\lambda}(\varphi_\mu) = \lambda\,\frac{d^5\Sigma^+ - d^5\Sigma^-}{d^5\Sigma^+ + d^5\Sigma^-} = \frac{\lambda\, d^5\widetilde{\Sigma}_{\mathcal{I}_2}}{d^5\Sigma_{BH_1} + d^5\Sigma_{BH_2} + d^5\Sigma_{BH_{12}} + d^5\Sigma_{DDVCS} + d^5\Sigma_{\mathcal{I}_1} + d^5\Sigma_{\mathcal{I}_2}} \tag{30}$$

$$A_{LU}^{S^\lambda} \propto \Im\mathfrak{m}\left\{F_1\mathcal{H} + \xi'(F_1+F_2)\widetilde{\mathcal{H}} - \frac{t}{4M_N^2}F_2\mathcal{E}\right\}$$

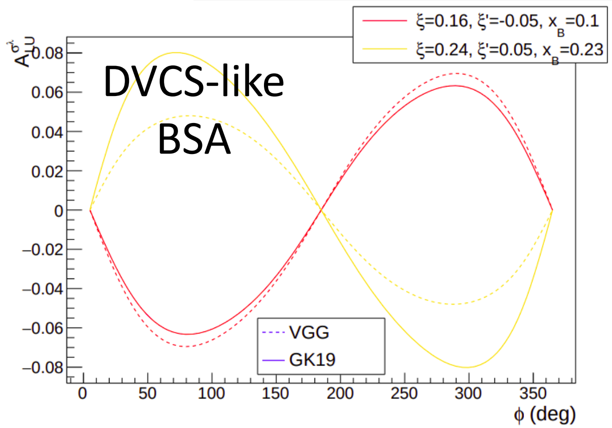

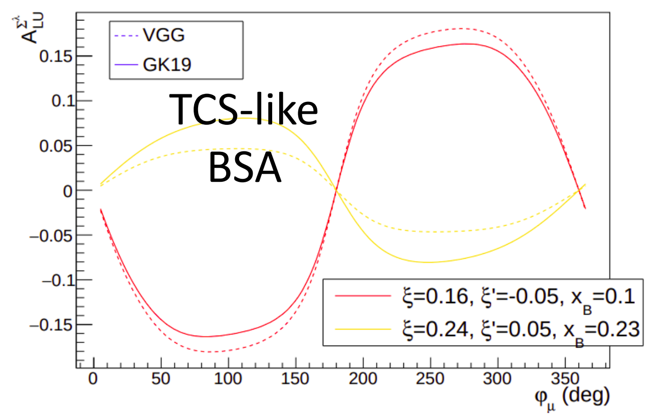

- Access to the imaginary part of CFFs
- Sign change when transitioning from DVCS region ($\xi'>0$, $Q^2>Q'^2$) to TCS region ($\xi'<0$, $Q^2<Q'^2$)
- TCS(DVCS)-like BSA enhances the amplitude in the $\xi'<0$($\xi'>0$) region
- **DDVCS BSAs** are **dominated** by the CFF **H** as DVCS and TCS, thus providing a similar quality measurement of the **H** GPD at $\xi' \neq \pm\xi$

Muon Charge Asymmetry

$$A_{UU}^{FB}(\varphi_\mu) = \frac{d^5\Sigma_{UU}(\varphi_{\mu^-}) - d^5\Sigma_{UU}(\varphi_{\mu^-}+\pi)}{d^5\Sigma_{UU}(\varphi_{\mu^-}) + d^5\Sigma_{UU}(\varphi_{\mu^-}+\pi)} = \frac{d^5\Sigma_{UU}(\varphi_{\mu^-}) - d^5\Sigma_{UU}(\varphi_{\mu^+})}{d^5\Sigma_{UU}(\varphi_{\mu^-}) + d^5\Sigma_{UU}(\varphi_{\mu^+})} = A_{UU}^{\mu^\pm}(\varphi_\mu)$$

$$\begin{aligned} d^5\Sigma_{UU}(\varphi_{\mu^-}+\pi) &= \int_0^{2\pi} d\phi \int_{\pi/2-\theta_0}^{\pi/2+\theta_0} d\theta_{\mu^-}\sin(\theta_{\mu^-}) \frac{d^7\sigma^0(\phi, \pi-\theta_{\mu^-}, \varphi_{\mu^-}+\pi)}{dx_B\, dy\, dt\, d\phi\, dQ'^2\, d\Omega_{\mu^-}} \\ &= \int_0^{2\pi} d\phi \int_{\pi/2-\theta_0}^{\pi/2+\theta_0} d\theta_{\mu^+}\sin(\theta_{\mu^+}) \frac{d^7\sigma^0(\phi, \theta_{\mu^+}, \varphi_{\mu^+})}{dx_B\, dy\, dt\, d\phi\, dQ'^2\, d\Omega_{\mu^+}} = d^5\Sigma_{UU}(\varphi_{\mu^+}) \end{aligned}$$

aka Forward Backward Asymmetry

$$A_{UU}^{\mu^\pm}(\varphi_\mu) = \frac{d^5\Sigma_{BH_{12}} + d^5\Sigma_{\mathcal{I}_2}}{d^5\Sigma_{BH_1} + d^5\Sigma_{BH_2} + d^5\Sigma_{DDVCS} + d^5\Sigma_{\mathcal{I}_1}}$$

$$d^5\Sigma_{\mathcal{I}_2} \propto -\frac{\xi'}{\xi}\Re\mathfrak{e}\left[F_1\mathcal{H} + \frac{\xi^2}{\xi'}(F_1+F_2)\tilde{\mathcal{H}} - \frac{t}{4M_N^2}F_2\mathcal{E}\right]$$

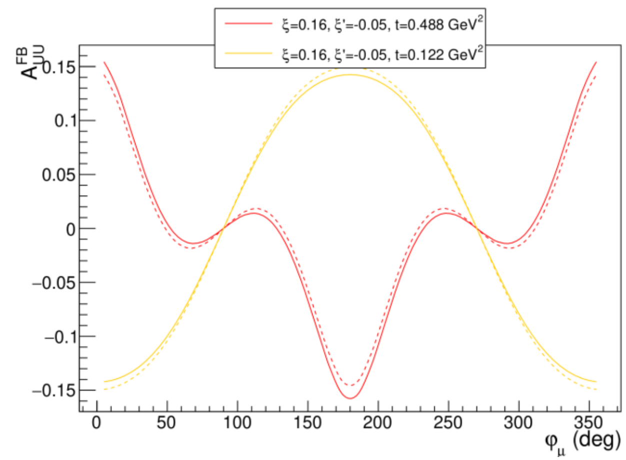

- Access to the real part of CFFs
- The Muon Charge Asymmetry (**μCA**), similar in nature to the forward-backward asymmetry of TCS, is predicted to have **significant amplitude** and rich **harmonic composition**
- Curvature sign change is a highly-discriminating feature for models
- **DDVCS μCA is dominated** by the CFF **H** and access a **CFF combination different** from **BSA**. This feature **distinguishes DDVCS** from DVCS and TCS

Experimental Setup

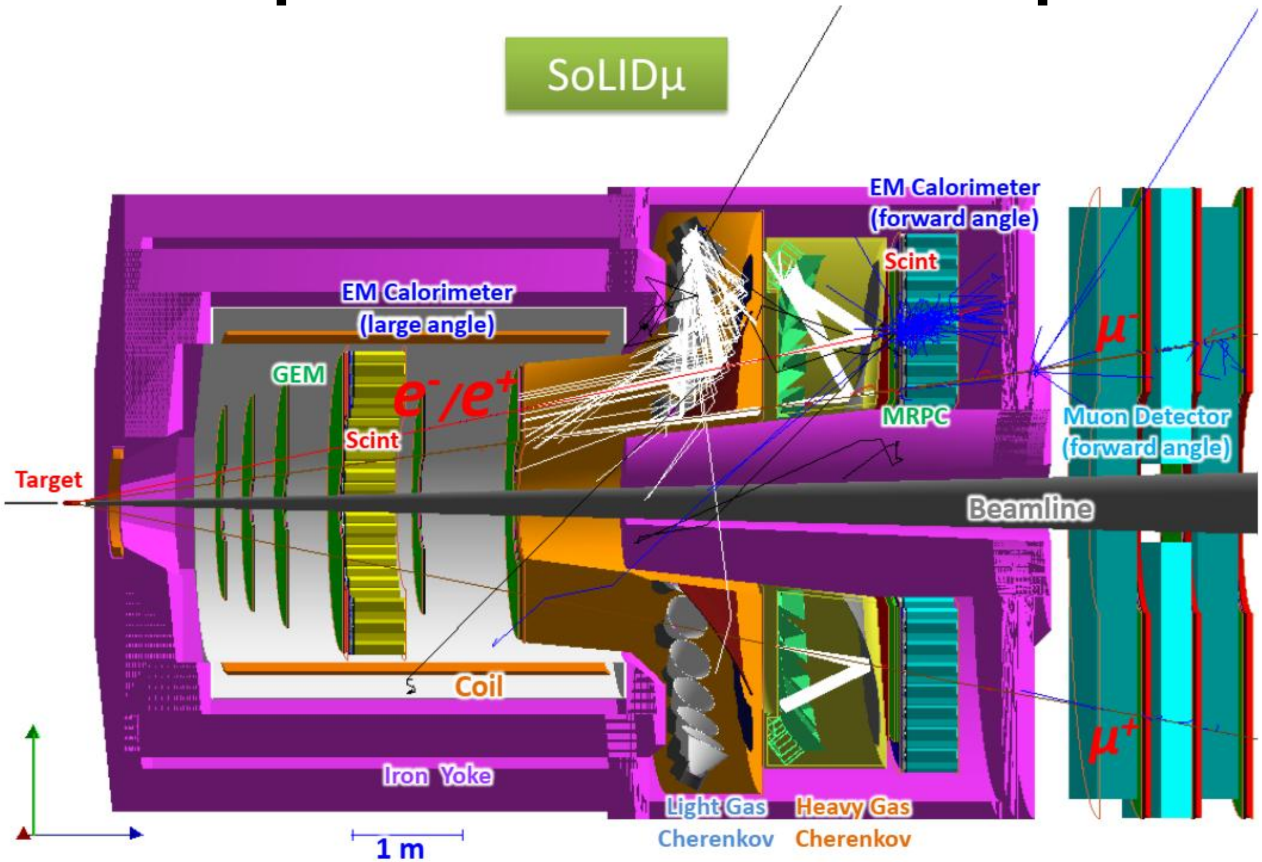

- Based on SoLID J/Psi and TCS setup with forward angle muon detector added to form SoLIDμ spectrometer
- Sharing beam time with added muon channels for J/Psi and TCS
- Forward Angle (FA) covers 8.5-16.5deg and Large Angle (LA) covers 18-30deg

Forward Angle Muon Detector (FAMD)

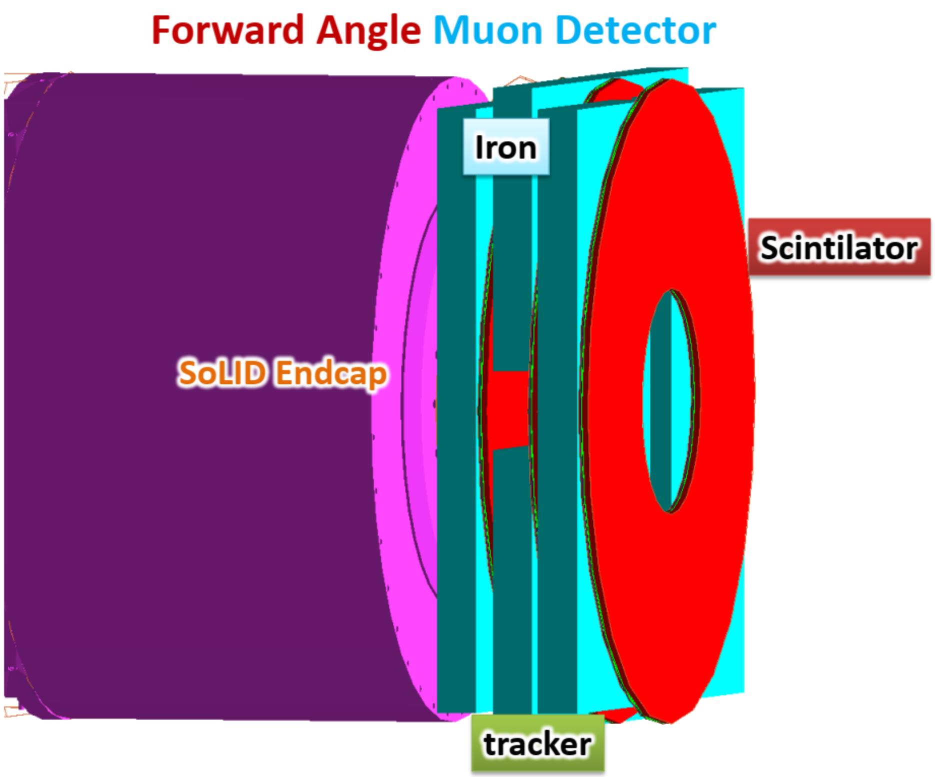

- 3 layers of iron for pion blocking
- 3 layers of µRWell trackers for tracks in FAMD to connect with tracks in SoLID inner GEM trackers
  - track resolution from SoLID inner trackers only
- 3 layers of scintillators for muon PID with pion suppression and for trigger

Iron of FAMD

- Reuse 6 of 8 CLEO octagon outer layer iron
- Each one is about 36x254x533cm
- No problem with space
- Field (<10G),force(<1N),torque(<2Nm) are small

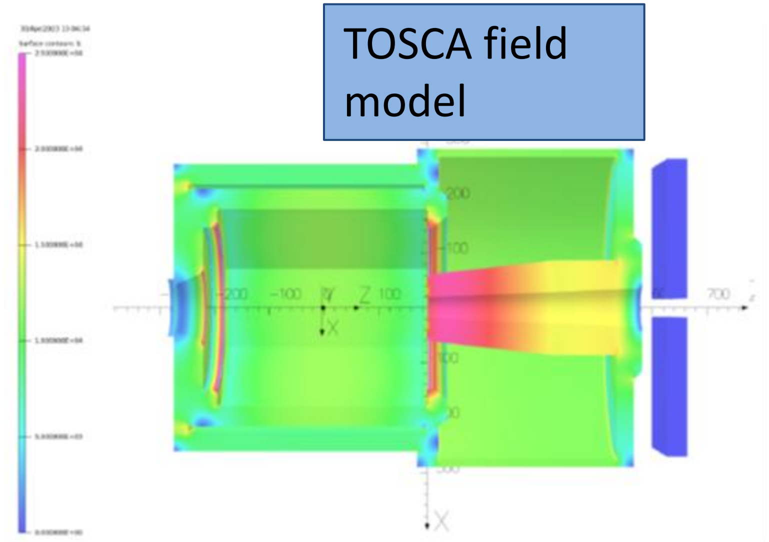

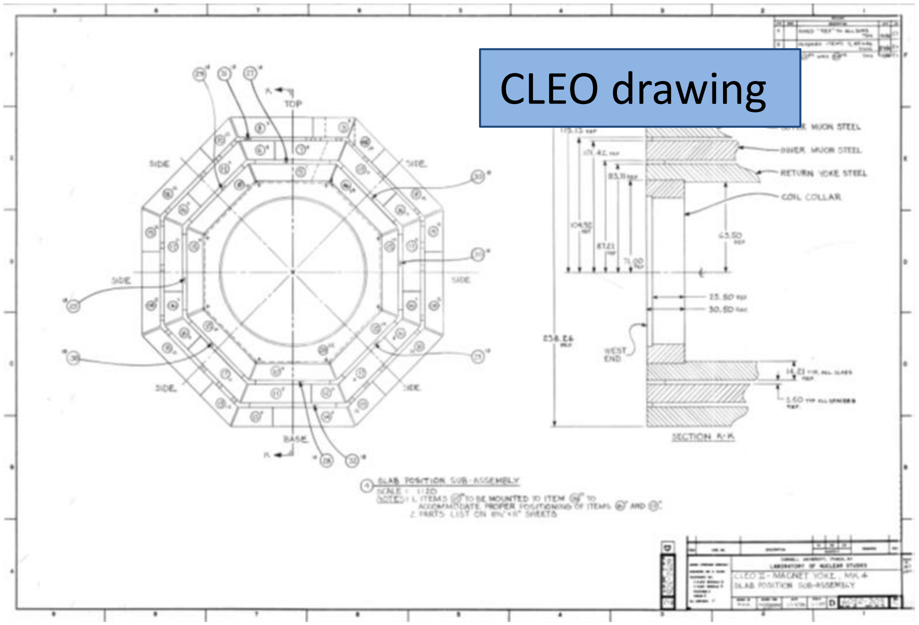

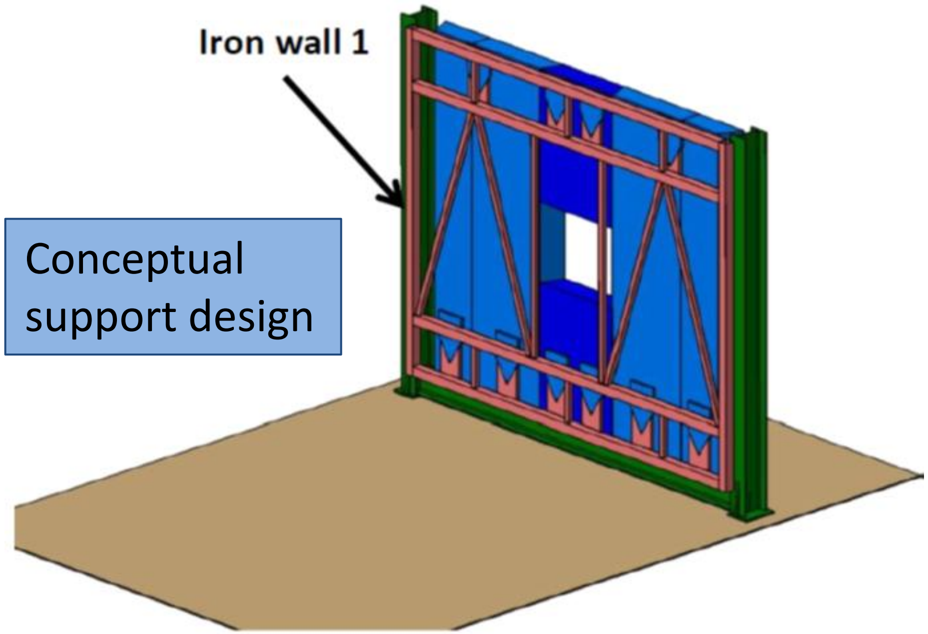

µRWell trackers of FAMD

- µRWell with good rate capability and lower cost than GEM
- VMM electronics
- 2D UV strips with capacitive charge sharing to have rate 30KHz/cm2 and position resolution of 1 mm

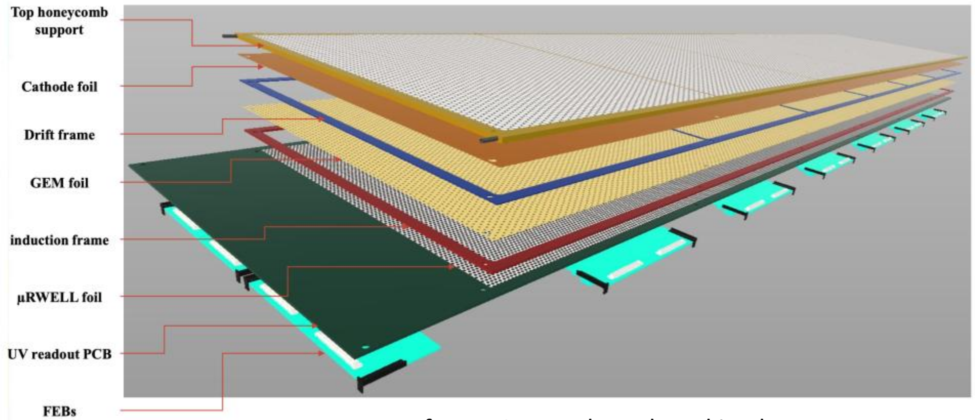

μRWELL Detector for EPIC outer barrel tracking layer

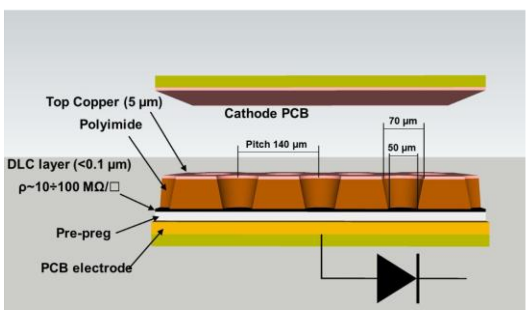

μRWELL Detector – G. Bencivenni *et al* 2019 *JINST* **14** P05014

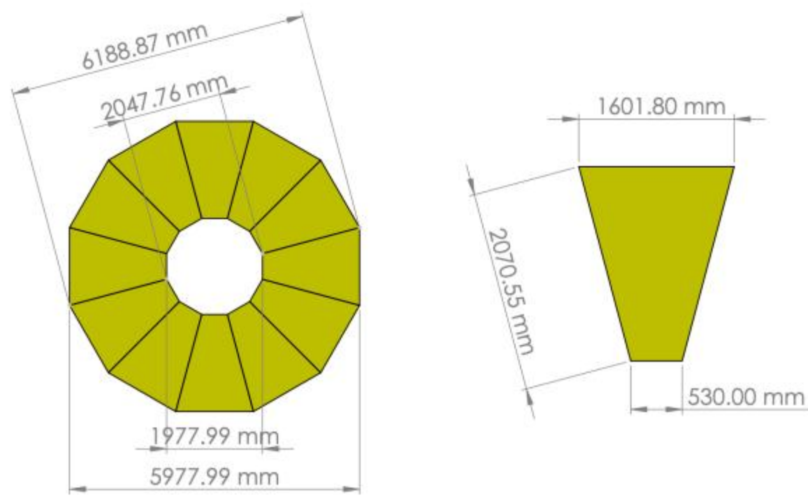

A plane of μRWELL detectors for muon detection

Scintillators of FAMD

- Each plane has 60 azimuthal segments
- Readout with light guide and PMTs from both inner and outer radial ends
- Thickness 5cm and 150 ps time resolution
- Design similar to CLAS12 forward scintillator and SoLID large angle scintillator with similar performance

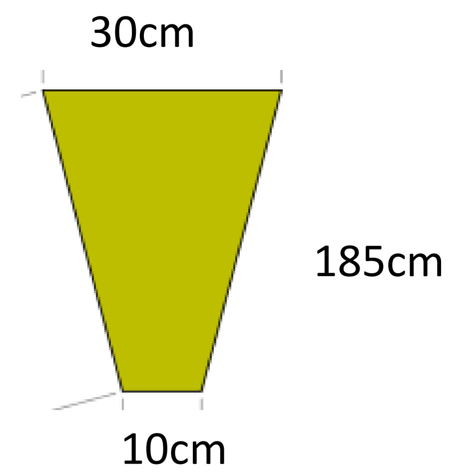

Event Acceptance

BH generator "grape-dilepton" used by HERA and verified by CLAS12

- Best topology 3fold(e+mu+mu): scattered e- at FA+LA, both muons at FA, proton not detected (shown below)
- Additional topology 4fold(e+mu+mu+p): scattered e- and recoil proton at FA+LA, both muons at FA

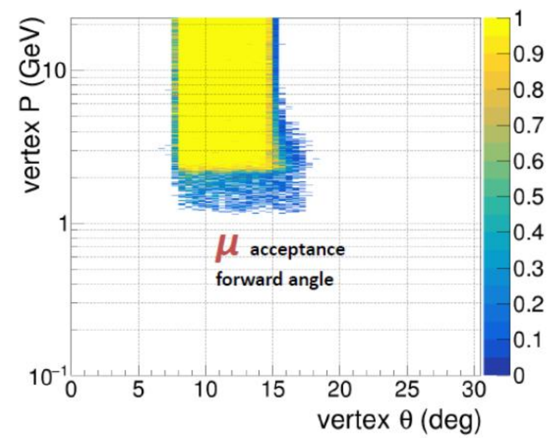

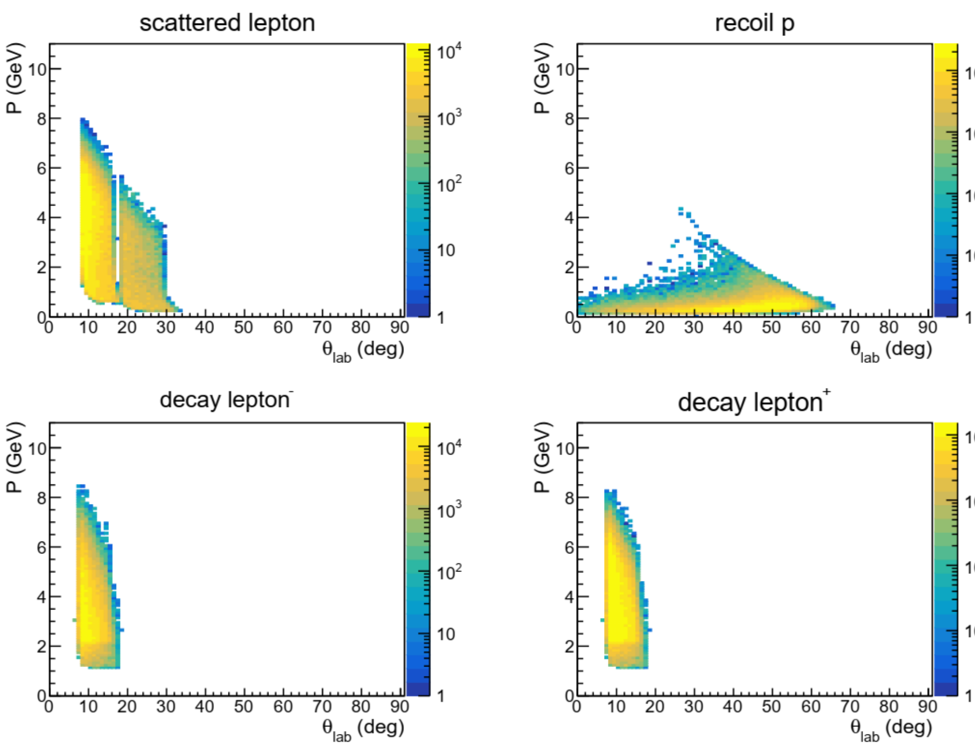

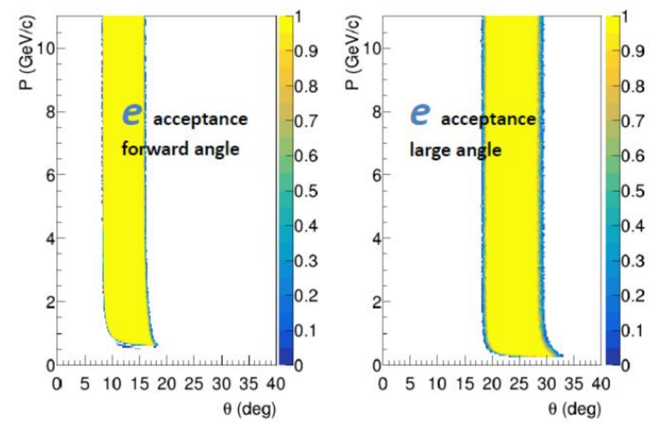

Event Distribution

BH generator "grape-dilepton" used by HERA and verified by CLAS12

- 3fold BH events covers large kinematic range
- 0.7 overall detection efficiency
- Enough counts for 1.2e37/cm2/s lumi and 100 days to have multidimensional binning

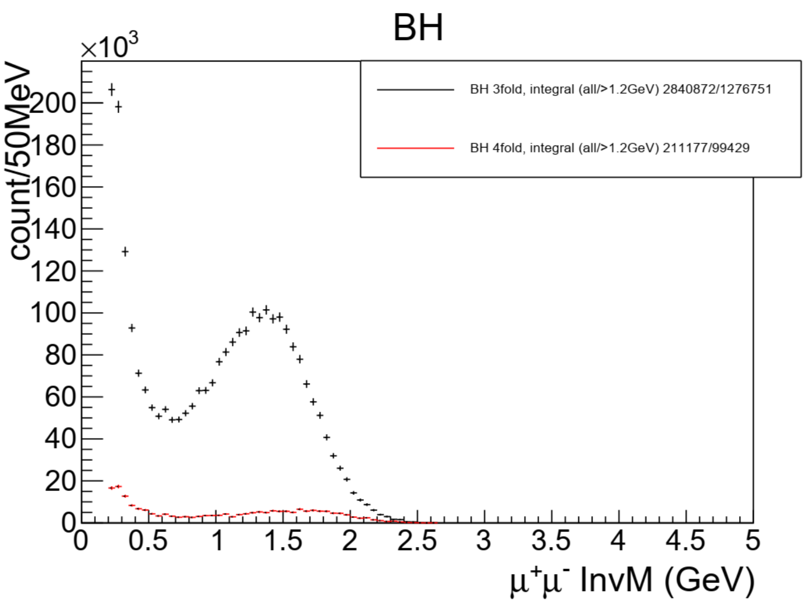

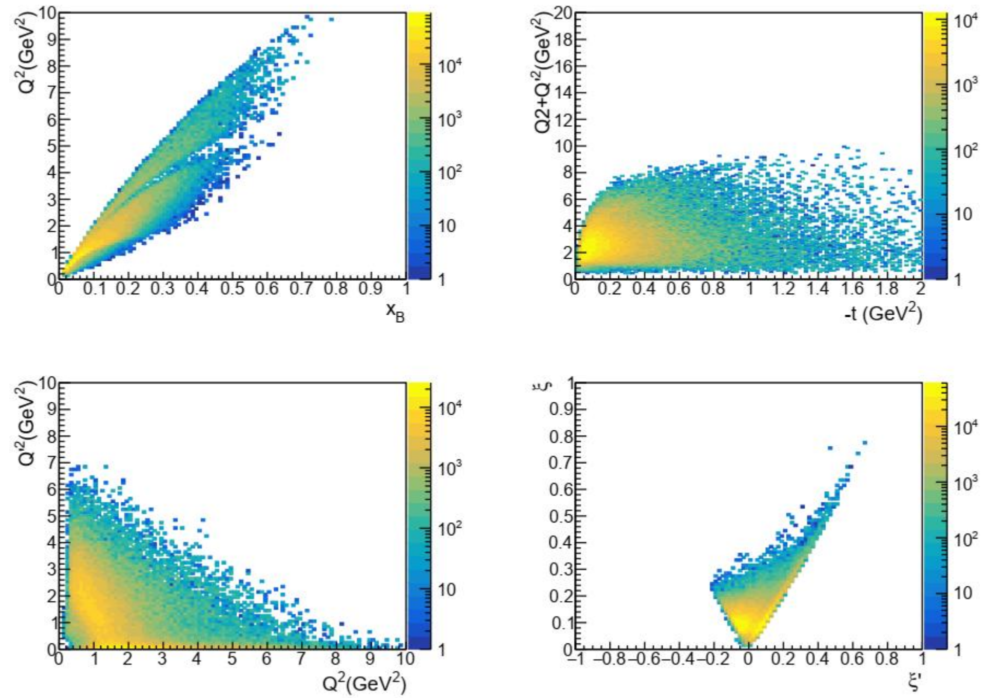

Exclusivity cut

- Both BH with 4 final particles (elastic) and more than 4 particles (quasi-elastic) are generated by "grape-dilepton"
- Missing proton mass of 3 fold BH events with resolution from SoLID inner GEM trackers, for resonance free region (muon pair InvM>1.2GeV)
- 3-4% background left after cutting MM>1.15GeV

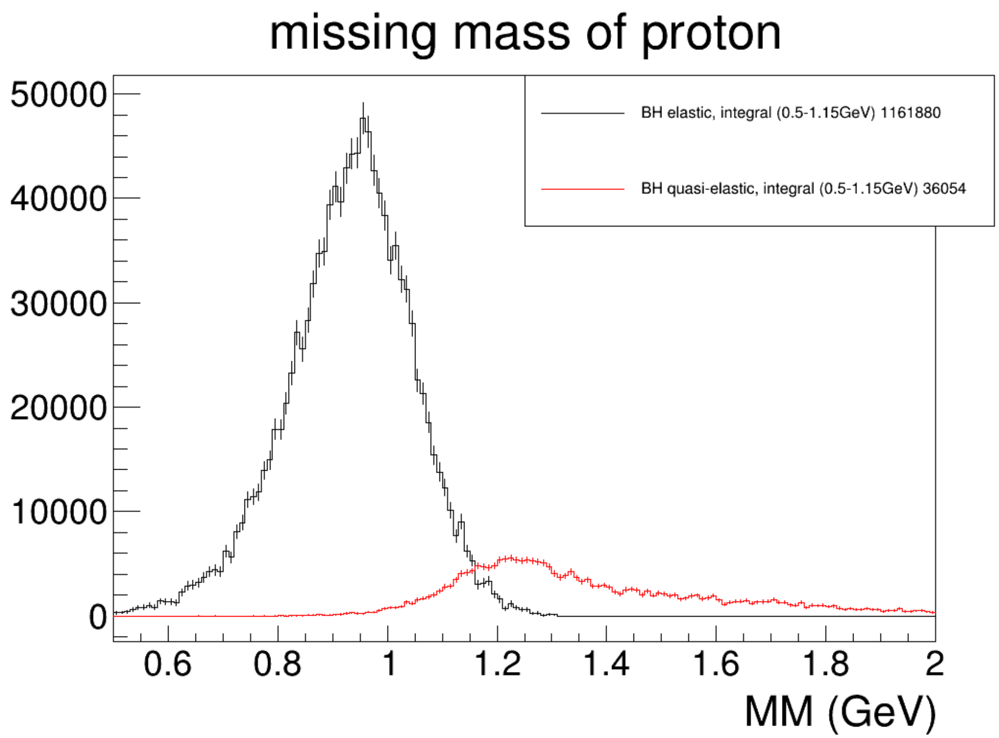

Pion blocking

- Geant4 simulation of pions from target with some probabilities creating hits at FAMD
- "pion hit probability", hits of charged particles entering each layer, used for FAMD detector and trigger rate estimate
- "pion surviving probability", hits of pion and muon at the last layer of FAMD and a track passing all SoLID inner GEM trackers, used for physics event rate estimation

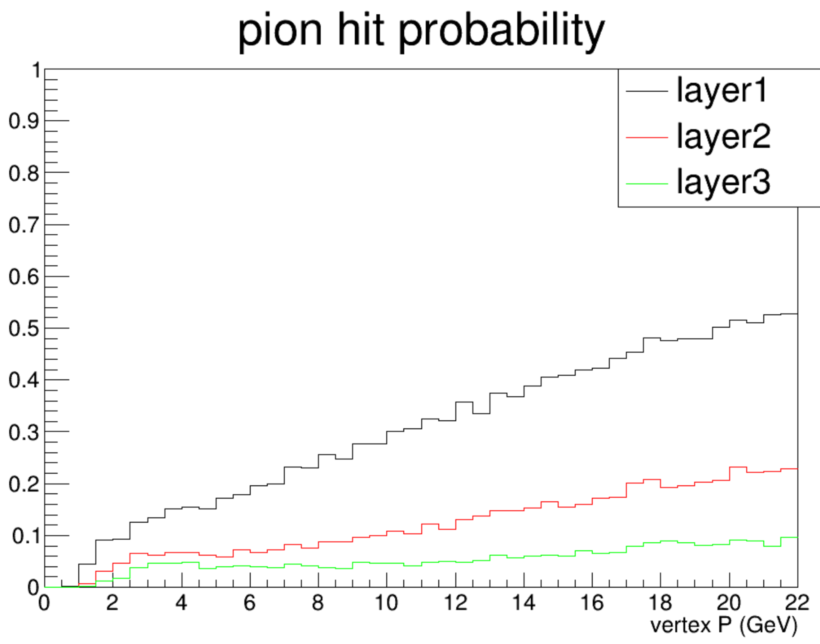

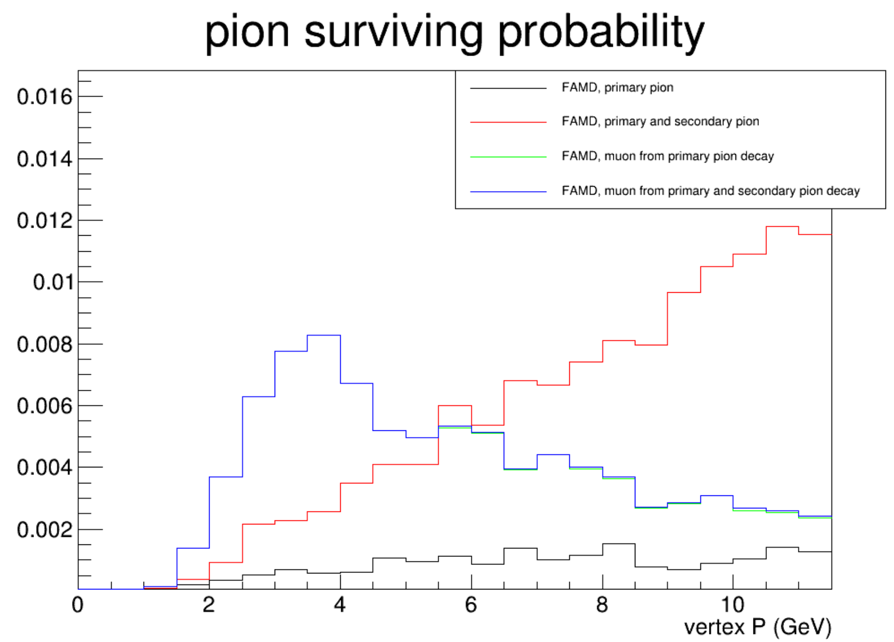

Pion suppression within FAMD

- Muons behave as Minimum Ionizing Particle (MIP)
- Pions often deposit more energy over 3 layers of scintillators.
- Use moderate pion suppression factor 2 from energy cut

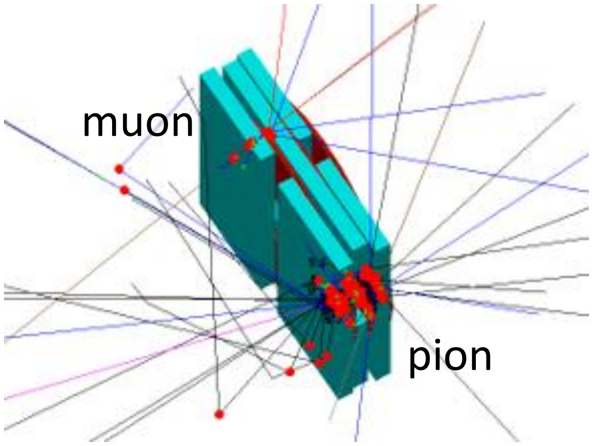

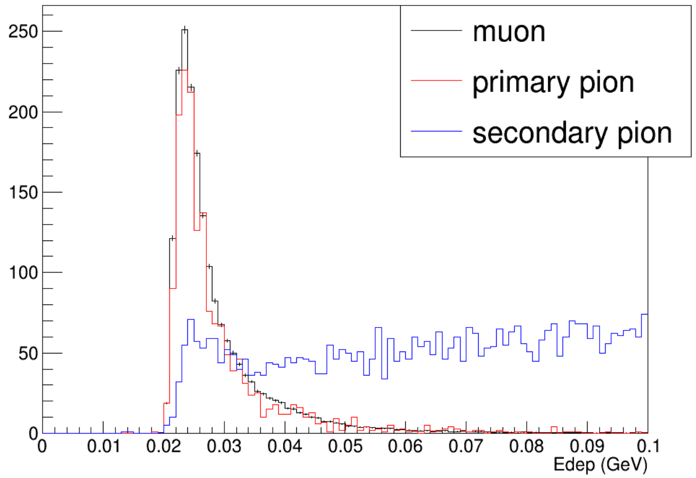

Single pion background

- Combining single pion generator "evgen_bggen" (pythia+MAID) events with "pion hit probability", study charged particle rate at 3 layers. Full simulation confirmed the result
- Single particle trigger 600khz rate with hits in all 3 layers of scintillators in nearby phi sectors
- Coincidence of two hits from 2 single particle trigger from 2 different phi sectors within 50ns time windows leads to 18khz final trigger rate
- Fake coin rate from single pion is below 1khz. BH di-muon events have two muons separated at least by 60 degrees in phi angle for the main physics region (muon pair InvM>1.2GeV)

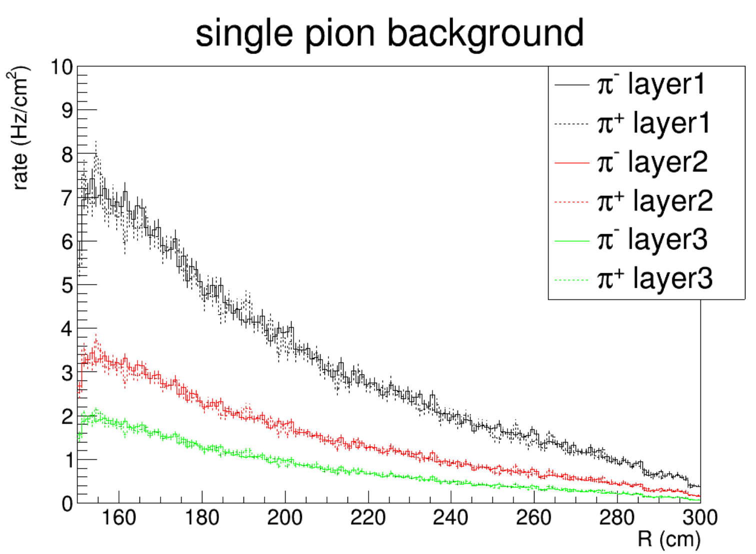

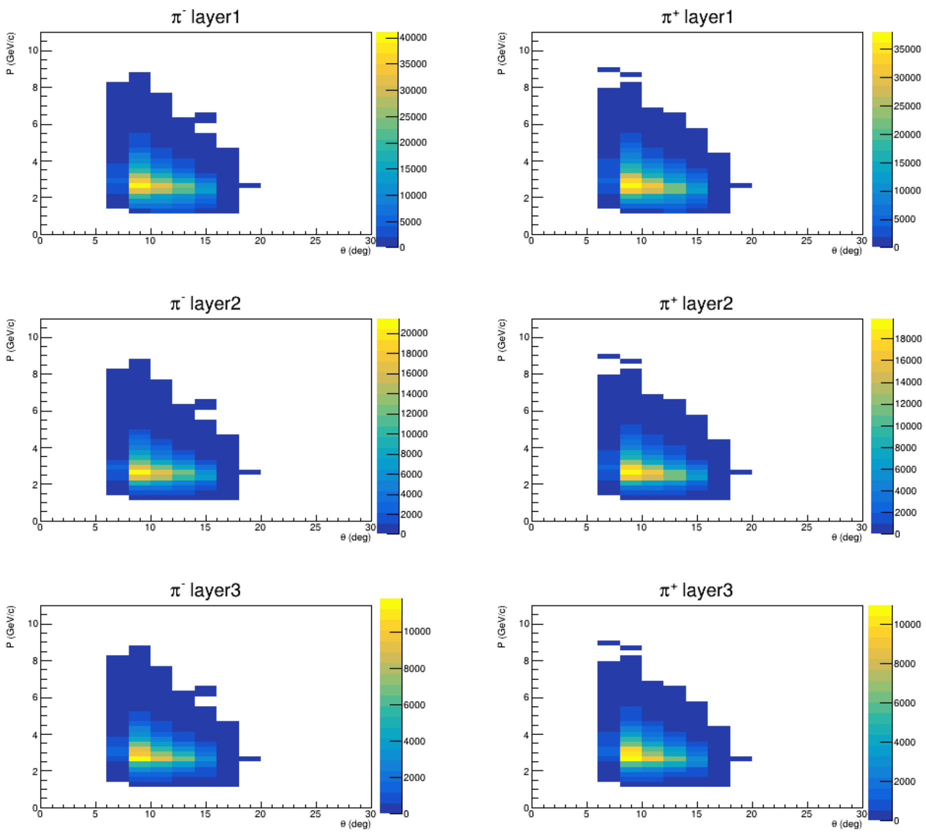

Two pion exclusive background

- Main physics background from two pion exclusive channel (missing mass cut won't reject it because pions and muons have similar mass)
- Combine event generator "twopeg" (fit to CLAS data) and "pion hit probability" with pion suppression factor 2, study "2pi" rate and compare to BH rate
- 5-7% background

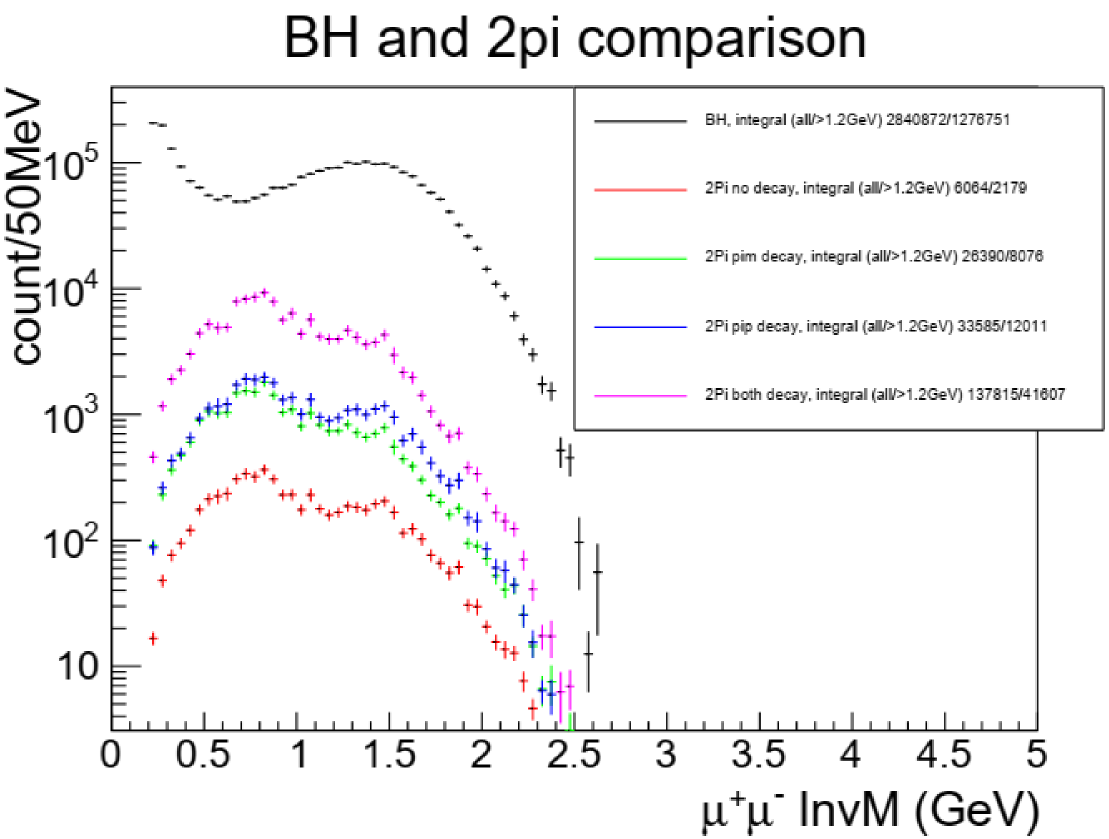

Experimental projections

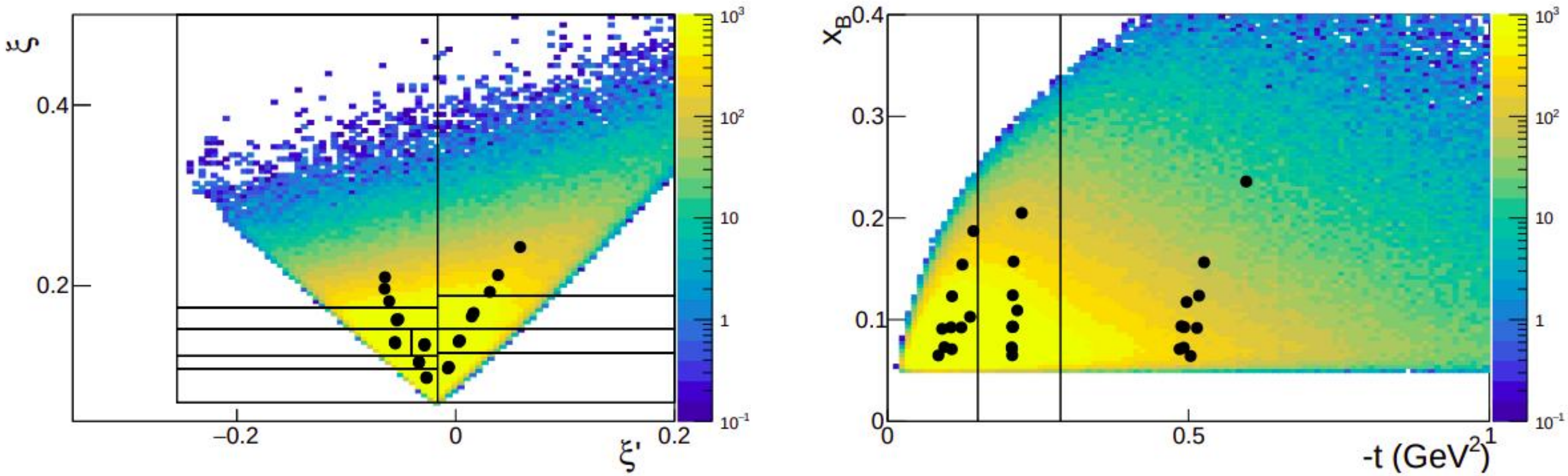

(a) (ξ', ξ) space.

(b) $(-t, x_B)$ space.

- 100 days would allow for measurements on a five-dimensional grid

BSA experimental projections

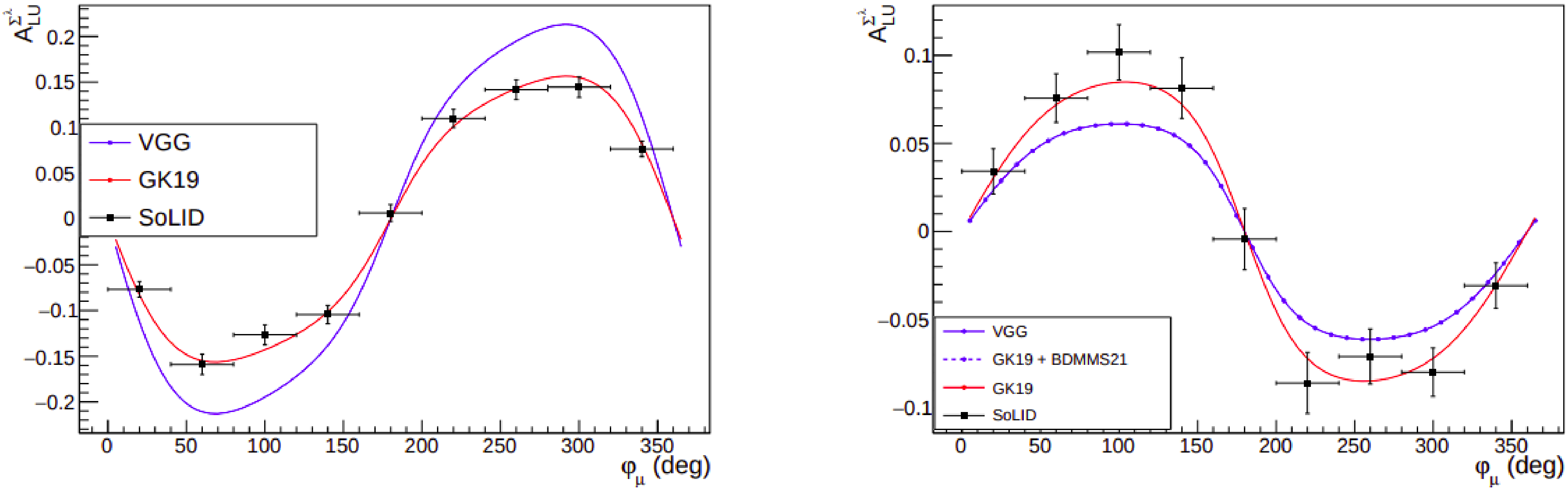

(a) TCS-like BSA in the TCS-like region (Bin 21).

(b) TCS-like BSA in the full DVCS-like region.

Figure 25: Sample TCS-like BSA projections.

- First time measurements of the BSA sign change
- Possibility to constrain GPD models

BSA experimental projections

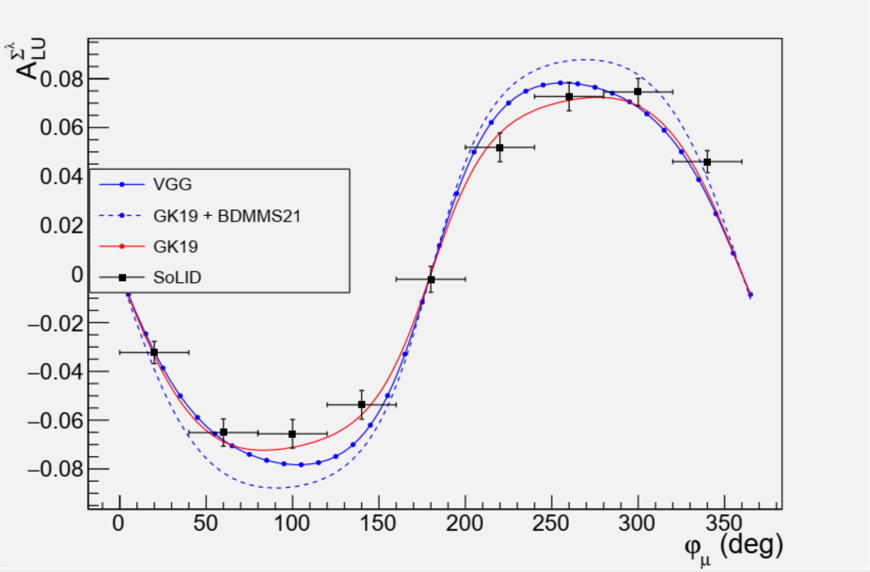

(a) $-0.1 < \xi' < -0.04$.

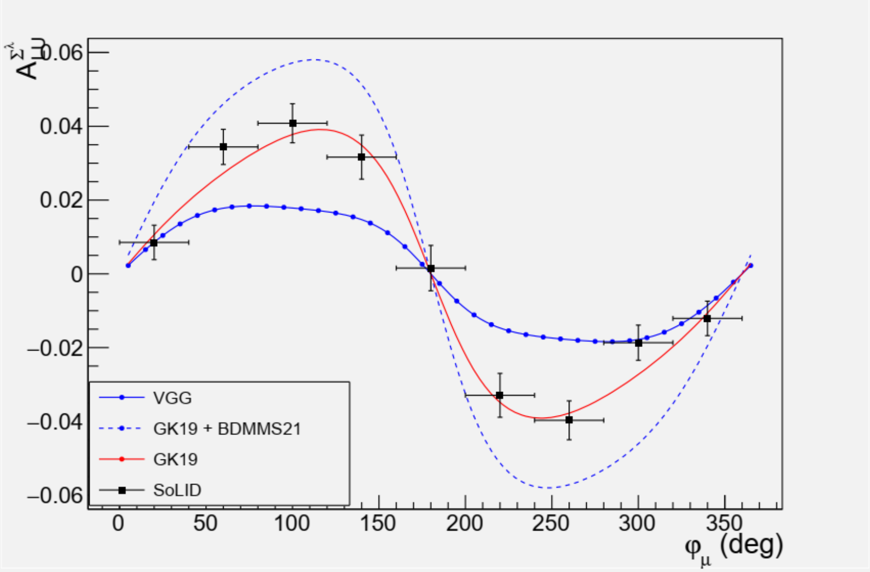

(b) $-0.04 < \xi' < 0.1$.

Figure 26: Projected exploratory TCS-like BSA measurements sensitive to shadow GPDs in the $0.3 < \xi < 0.4$ region.

- First-time exploratory measurement constraining shadow GPD models

μCA experimental projections

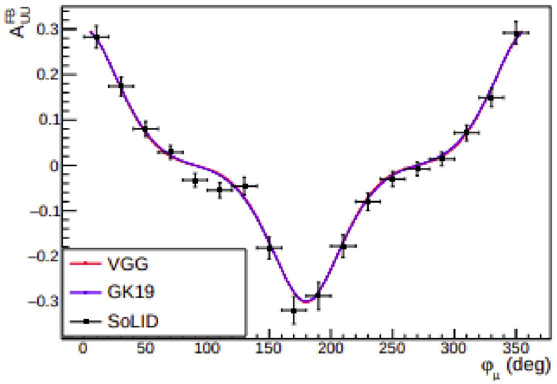

(d) Bin 19.

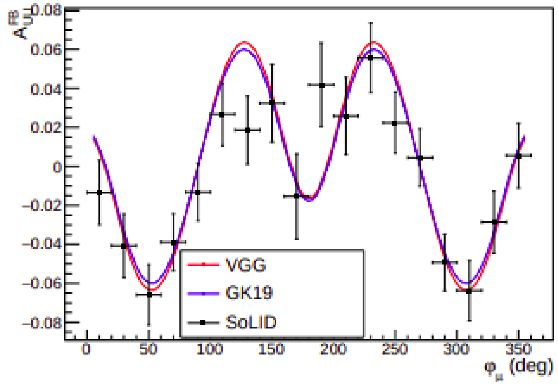

(e) Bin 20.

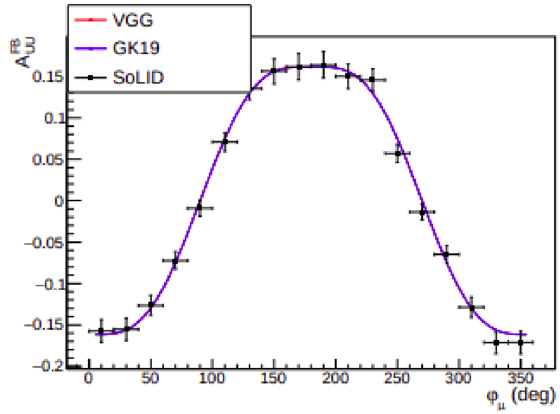

(f) Bin 21.

- Observation of the CFF real part with curvature change

μCA experimental projections

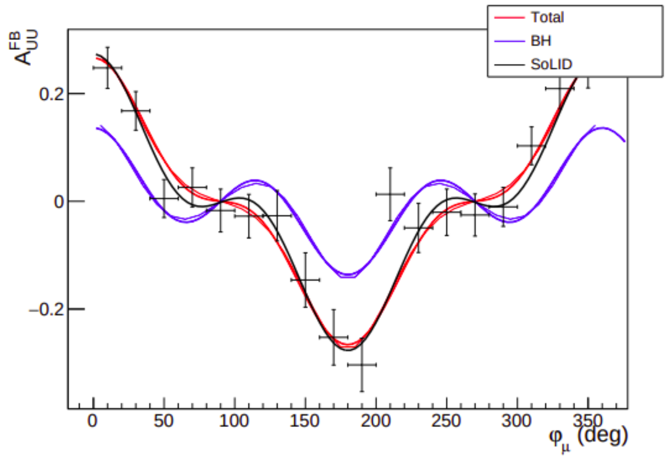

(a) μCA and the components entering the $\cos\varphi_\mu$ moment.

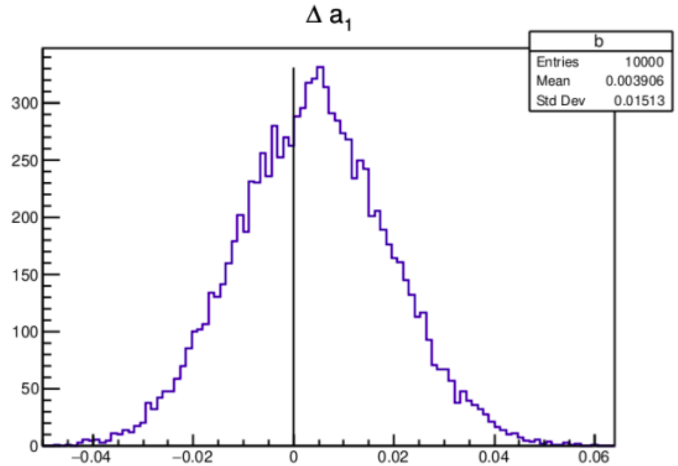

(b) Distribution of the $\cos\varphi_\mu$ moment of the μCA after 10k iterations.

Figure 28: Extraction of $\cos\varphi_\mu$ moment of the μCA on bin 13.

Sample cos(ϕ) extraction with a 11% error

$$A_{UU}^{FB} = a_0 + a_1\cos(\varphi) + a_3\cos(3\varphi)$$

- μCA has contributions from cos(ϕ) and cos(3ϕ) modulations
- cos(ϕ) can be extracted from fits
- As BH is known, it can be subtracted

$$\frac{d^4\sigma_{INT}}{dQ'^2 dt d\Omega} = -\frac{\alpha_{em}^3}{4\pi s^2}\frac{1}{-t}\frac{m_p}{Q'}\frac{1}{\tau\sqrt{1-\tau}}\frac{L_0}{L}[\cos(\phi)\frac{1+\cos^2(\theta)}{\sin(\theta)}\mathrm{Re}\tilde{M}^{--}$$
$$\cancel{-\cos(2\phi)\sqrt{2}\cos(\theta)\mathrm{Re}\tilde{M}^{0-}} + \cos(3\phi)\sin(\theta)\mathrm{Re}\tilde{M}^{+-} + O(\frac{1}{Q'})],$$

Systematic effects

The definition of experimental observables at the 5-fold differential level is required to compensate the cross-section smallness and to minimize the contribution of the BH_2 process

$$\boxed{A_{LU}^{\Sigma\lambda} = \frac{1}{\lambda} \frac{Y_+ - Y_-}{Y_+ + Y_-}} \quad Y_\pm(\varphi_\mu) = \frac{1}{Q_\pm} \frac{1}{\Delta\Omega_e(\varphi_\mu)\, \Delta\theta_\mu(\varphi_\mu)} \int_0^{2\pi} d\phi \int_{\pi/4}^{3\pi/4} d\theta_\mu \sin(\theta_\mu) \frac{N_\pm(\varphi_\mu, \phi, \theta_\mu)}{\boldsymbol{\epsilon_e}(\phi)\, \boldsymbol{\epsilon_\mu}(\varphi_\mu, \theta_\mu)}$$

$$\boxed{A_{UU}^{\mu^\pm} = \frac{Y^+ - Y^-}{Y^+ + Y^-}} \quad Y^\pm(\varphi_\mu) = \frac{1}{\Delta\Omega_e(\varphi_\mu)\, \boldsymbol{\Delta\theta_{\mu^\pm}}(\varphi_\mu)} \int_0^{2\pi} d\phi \int_{\pi/4}^{3\pi/4} d\theta_\mu \sin(\theta_\mu) \frac{N^\pm(\varphi_\mu, \phi, \theta_\mu)}{\boldsymbol{\epsilon_e}(\phi)\, \boldsymbol{\epsilon_{\mu^\pm}}(\varphi_\mu, \theta_\mu)}$$

- BSA systematics originates from the knowledge of : the electron beam polarization, the electron detection efficiency, and the muon detection efficiency.
- μCA systematics originates from the knowledge of : the electron detection efficiency, the muon detection efficiency, and the muon solid angle.

Systematic effects

- Systematics of the measurements will be controlled via **simulations** and the measurement of **reference processes**. The **solenoidal field** and the **symmetrical configuration** of SoLIDμ offer further cross-checks
- **Muon solid angle** : extensive simulations based on the **SoLIDμ GEANT4 model** ($\delta\Delta\theta_\mu/\Delta\theta_\mu \sim 3\%$)
- **Electron detection efficiency** : measurement of **DIS** and **elastic** electron **scattering** ($\delta\epsilon_e/\epsilon_e \sim 7\%$)
- **Muon detection efficiency** : measurement of **Bethe-Heitler** and comparison of the $\boldsymbol{e^\pm}$ and $\boldsymbol{\mu^\pm}$ **decay** of specific meson (ϕ, J/Ψ) ($\delta\epsilon_\mu/\epsilon_\mu \sim 15\%$)

Bin independence hyptothesis

$$Y_\pm(\varphi_\mu) \equiv \sum_{i=1}^{N_\phi}\sum_{j=1}^{N_{\theta_\mu}} \frac{n_\pm^{ij}}{\epsilon_e^i\,\epsilon_\mu^j}$$

$$\boxed{\delta A_{LU}^{\Sigma\lambda} = \sqrt{\left[A_{LU}^{\Sigma\lambda}\right]^2\left(\frac{\delta\lambda}{\lambda}\right)^2 + \frac{1}{2\lambda^2}\frac{1}{N_\phi}\left(\frac{\delta\epsilon_e}{\epsilon_e}\right)^2 + \frac{1}{2\lambda^2}\frac{1}{N_{\theta_\mu}}\left(\frac{\delta\epsilon_\mu}{\epsilon_\mu}\right)^2}} \rightarrow \mathbf{0.04}$$

λ = 0.85

$$Y^\pm(\varphi_\mu) \equiv \frac{1}{\Delta\theta_{\mu^\pm}}\sum_{i=1}^{N_\phi}\sum_{j=1}^{N_{\theta_\mu}} \frac{n_{ij}^\pm}{\epsilon_e^i\,\epsilon_{\mu^\pm}^j}$$

$$\boxed{\delta A_{UU}^{\mu^\pm} = \sqrt{\left(\frac{\delta\Delta\theta_\mu}{\Delta\theta_\mu}\right)^2 + \frac{1}{N_\phi}\left(\frac{\delta\epsilon_e}{\epsilon_e}\right)^2 + \frac{1}{N_{\theta_\mu}}\left(\frac{\delta\epsilon_\mu}{\epsilon_\mu}\right)^2}} \rightarrow \mathbf{0.06}$$

(N_ϕ, N_{θ_μ}) *are the kinematic dependent number of bins, typically (20,10)*

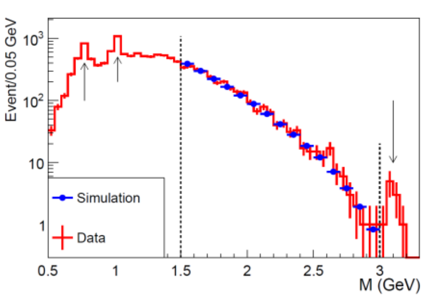

- CLAS12 di-e data and sim of BH in resonance free region are used to check absolute efficiency and its error.
- GlueX has done similar thing
- SoLIDμ should use both resonance and resonance free region and cross check both di-e and di-mu channels to help systematics study

Beam time request

Beam Energy (GeV)	Beam Current (uA)	Beam Requirements	Target Material	Target Thickness (cm)	Beam time (days)
11	3	polarized (>85%)	LH2	15	
Run Group Calibration time					10
Run Group Production time					50
Requested Production time					50
Total Time					110

- Only trigger on di-muon to take DDVCS, J/Psi and TCS di-mu data at the same time
- Independent di-e data taking happening at the same time

Summary

- complement SoLID J/Psi setup with a forward angle muon detector to form SoLIDμ spectrometer
- measure DDVCS in the di-muon channel
- use the J/Psi beamtime 60 days and request additional 50 days
- first time measurement of DDVCS (mainly BSA, and exploratory μCA) over a broad kinematic range
- first time to access GPD $|x| < \xi$ as input for models
- J/Psi and TCS will have additional di-muon data and more di-e data